Single-Walled MoTe 2 Nanotubes

ARTICLE *in* NANO LETTERS · NOVEMBER 2007

Impact Factor: 13.59 · DOI: 10.1021/nl071165+ · Source: PubMed

3 AUTHORS, INCLUDING:

Xiaojun Wu
University of Science and Technology of China
116 PUBLICATIONS **2,342** CITATIONS
SEE PROFILE

Zhanping Xu
University of Nebraska at Lincoln
7 PUBLICATIONS **29** CITATIONS
SEE PROFILE

NANO LETTERS

2007
Vol. 7, No. 10
2987−2992

Single-Walled $MoTe_2$ Nanotubes

Xiaojun Wu, Zhanping Xu, and X. C. Zeng*

Department of Chemistry and Nebraska Center for Materials and Nanoscience, University of Nebraska-Lincoln, Lincoln, Nebraska 68588

Received May 17, 2007

ABSTRACT

The structural, electronic, and mechanical properties of single-walled $MoTe_2$ nanotubes are investigated using density functional theory. All large-diameter $MoTe_2$ nanotubes are found to be narrow-gap semiconductors, whereas small-diameter nanotubes are found to be less stable compared to large-diameter nanotubes. Notably, the armchair $MoTe_2$ nanotubes exhibit an indirect band gap, whereas the zigzag nanotubes exhibit a direct band gap. The band gap decreases with decreasing diameter of the tube or if the tube is under compression or elongation in the axial direction. Young's modulus of $MoTe_2$ nanotubes is calculated and is found to be dependent on the diameter and chirality of the tubes. The armchair nanotubes are stiffer than the zigzag nanotubes with the same diameter. Compared to the homologous MoS_2 nanotubes, the $MoTe_2$ nanotubes are softer due to less strain-energy cost in forming the nanotube structures.

Introduction. As a member of layered transition-metal dichalcogenide compounds, MX_2 (M = Mo, W, Ta, or Nb, and X = S, Se, or Te), molybdenum ditelluride ($MoTe_2$) compounds, together with molybdenum dichalcogenide (MoS_2 and $MoSe_2$) compounds, have attracted increasing research attention because of their novel properties and potential applications. In these compounds, one layer of metal M is sandwiched between two layers of X, and the triple layers stack together through weak van der Waals interactions.[1,2] This layered structure enables molybdenum dichalcogenides electrically and mechanically anisotropic. For example, a nonlinear electrical behavior of bulk $MoTe_2$ single crystals has been revealed experimentally.[3] Molybdenum dichalcogenides are indirect semiconductors with their optical band gap comparable to the solar wavelength. Thus, molybdenum dichalcogenides hold promise in photovoltaic applications, such as electrodes in high-efficiency photoelectrochemical cells.[4−7] Moreover, Vellinga et al. reported a phase transition from semiconducting α-$MoTe_2$ to metallic β-$MoTe_2$.[12] Molybdenum dichalcogenides are also good solid lubricants, especially in extremely high-temperature environments and can be used as a fuel in nuclear reactors.[8] Molybdenum dichalcogenides can be intercalated with guest atoms. For example, the intercalation of lithium in MoS_2 has prompted application in lithium batteries.[9] Also, n-type and p-type $MoTe_2$ crystals can be fabricated through controlling the transport agent during the growth. Fabrication of p−n diodes of $MoTe_2$ has been reported.[10,11]

The discovery of carbon nanotubes (CNTs) has opened up an entirely new field of one-dimensional nanotube materials.[13−17] Single-walled CNTs can be viewed as the rolling up of a graphene sheet. The electronic properties of the CNTs are strongly dependent on their chirality, that is, how the graphene sheet is rolled up. Since the discovery of CNTs, considerable efforts have been devoted to synthesizing other forms of inorganic nanotubes as well as exploration of their properties and applications.[18−53] Most inorganic nanotubes can also be viewed as rolling up some layered structure analog to the graphite. For example, boron nitride nanotubes (BNNTs), synthesized shortly after the discovery of CNTs, can be viewed as rolled up hexagonal boron nitride layers. Subsequent studies of BNNTs have shown that the electronic properties of BNNTs are only weakly dependent on their chirality and diameter. This unique electronic behavior of BNNTs has been exploited for various potential applications.[18−27] Another form of inorganic nanotubes can be synthesized based on transition-metal dichalcogenides MX_2.[28−53] In this form of inorganic nanotubes, strong mixed covalent−ionic bonds exist within the layers while the stacked multilayers are held together through weak van der Waals forces. The first inorganic nanotubes of this form were WS_2, discovered by Tenne et al. in 1992,[28] followed by the finding of MoS_2 nanotubes.[29] Later, several catalyst- or template-based methods were developed to synthesize various inorganic nanotubes, including MoS_2,[29,30] WS_2,[28,31] WSe_2,[32] NbS_2,[33] TaS_2,[33] $NiCl_2$,[34] SnS_2/SnS,[35] HfS_2,[36] V_2O_5,[37] CdS/CdSe,[38] and TiO_2.[39,40] Subsequent experimental and theoretical studies of these inorganic nanotubes have revealed many new properties, particularly their novel tribological properties.[41−50] WS_2 nanotubes have also been tested as the tips of scanning-probe microscopes for the study of photostimulated processes on surfaces.[41] Recently, molybdenum ditelluride ($MoTe_2$) nanotubes have been synthesized in the laboratory.[51−53] In this paper, we report a comprehensive study of the structural, electronic, and mechanical properties

* Corresponding author. E-mail: xczeng@phase2.unl.edu.

10.1021/nl071165+ CCC: $37.00
Published on Web 08/29/2007

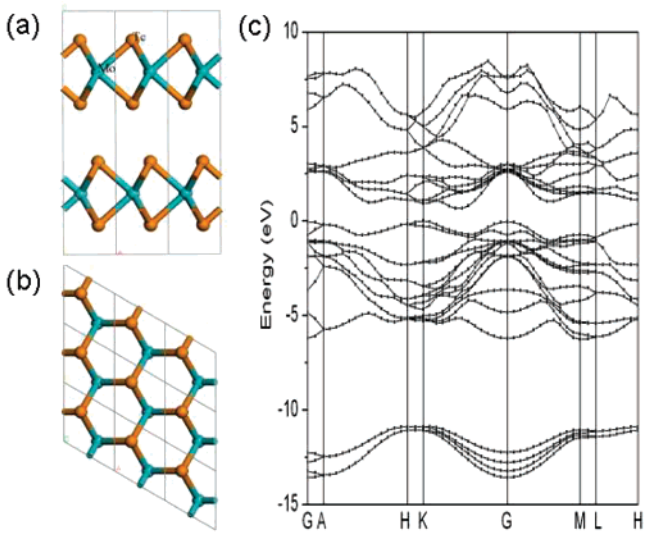

Figure 1. (a) Side and (b) top view of the layered structure of bulk $MoTe_2$. Mo atoms are blue, and Te atoms are in orange. (c) Calculated band structures of bulk $MoTe_2$. The Fermi energy level is set as zero.

of single-walled $MoTe_2$ nanotubes by using density functional theory (DFT). We find that the electronic and mechanical properties of $MoTe_2$ nanotubes can be strongly dependent on their structures. To our knowledge, this is the first ab initio study of the $MoTe_2$ nanotubes.

Computation Methods. All calculations were carried out by using a linear combination of atomic orbitals and DFT method implemented in DMol3 package.[54] We employed the Perdew−Burke−Ernzerhof (PBE) functional within the generalized gradient approximation (GGA) and double numerical basis sets with polarization function (DNP).[55] The DNP basis sets are comparable to Pople's 6-31G* basis sets.[56] For Mo, the outer 14 electrons ($4s^2 4p^6 4d^5 5s^1$) were treated as valence electrons, whereas for Te the outer 16 electrons ($4d^{10} 5s^2 5p^4$) were treated as valence electrons. The core electrons of Mo and Te atoms were described by density-functional semicore pseudopotentials with relativistic effects.[57] These norm-conserving pseudopentials can be generated by fitting all-electron relativistic DFT results and contain a nonlocal contribution for each channel up to $l = 2$, as well as a nonlocal contribution to account for higher channels. The real-space global cutoff radius was set to 5.0 Å and the spin-restricted DFT was selected to obtain all results for this work. To simulate the nanotube with infinite length, a tetragonal supercell with size of $40 \times 40 \times c$ Å^3 was adopted with the length c being the periodicity of the tube (in the axial direction). The k-point sampling was employed using the Monkhorst−Pack scheme.[58]

Results and Discussion. The wall of a single-walled $MoTe_2$ nanotube exhibits a triple-layer structure, which consists of a Mo layer sandwiched between two Te layers (space group $P63/mmc$) as shown in Figure 1.[1] The three atomic layers stack together through van der Waals interaction. Within each atomic layer, the atoms form covalent−ionic bonds. The separation between two neighboring layers is about 6.98 Å. The Mo−Te bond length is 2.75 Å, and the thickness of the triple layer is about 3.71 Å. Our DFT calculation shows that the bulk $MoTe_2$ is a semiconductor with an indirect band gap of ~0.66 eV and a direct band gap of 2.66 eV at the G point, consistent with previous DFT calculations.[6] Charge analysis using the Hirshfeld method shows that each Te atom receives ~0.03 e from the Mo atom.

As discussed in the introduction, a single-walled $MoTe_2$ nanotube can be constructed by rolling up a $MoTe_2$ triple layer, similar to other transition-metal dichalcogenide nanotubes.[43,49,50] In Figure 2, we show two prototype $MoTe_2$

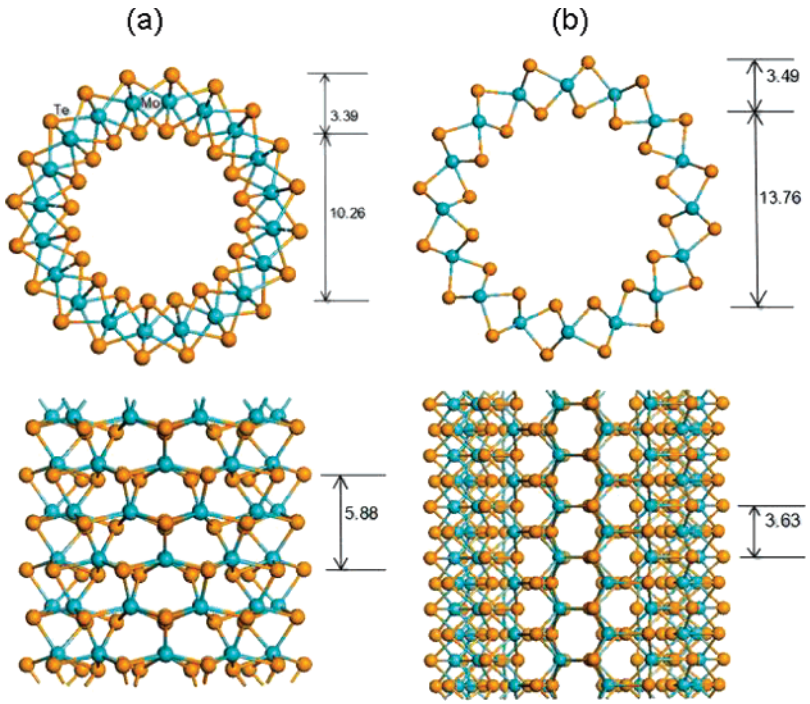

Figure 2. Top and side view of structures of (a) (10, 0) zigzag and (b) (8, 8) armchair $MoTe_2$ nanotubes.

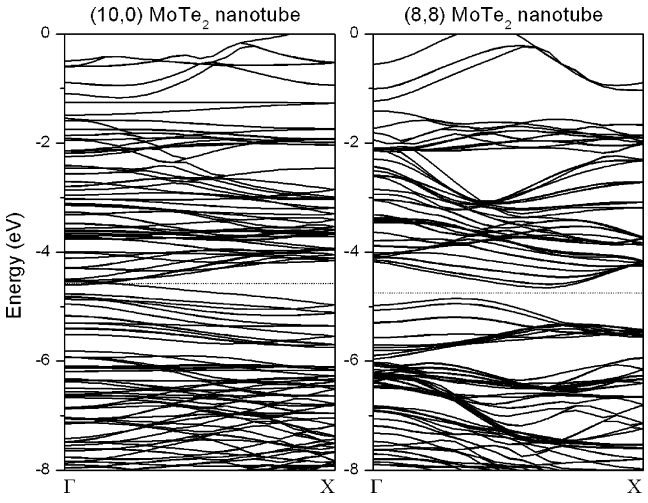

Figure 3. Calculated band structures of (10, 0) and (8, 8) $MoTe_2$ nanotubes. The Fermi level is labeled with a dotted line.

nanotubes: (a) the zigzag (10, 0) and (b) the armchair (8, 8) nanotubes. The unit-cell length in the axial direction is 5.88 and 3.63 Å, respectively for the two nanotubes. Because of the curvature effect, the formation of a tubular structure changes the Mo−Te bond lengths slightly. The thickness of a single wall is smaller than that of a perfect triple layer in the bulk. Meanwhile, the Mo−Te bonds in the outer layer are elongated, and some are shortened in the inner layer. For the (10, 0) tube, the Mo−Te bond lengths are 2.76, 2.95, and 2.95 Å in the outer layer and 2.69, 2.78, and 2.78 Å in the inner layer. For the (8, 8) nanotube, the bond lengths are 2.92, 2.81, and 2.81 Å in the outer layer and 2.76, 2.73, and 2.73 Å in the inner layer. The calculated band structures, as shown in Figure 3, indicate that the zigzag (10, 0) $MoTe_2$ nanotube is a metal, whereas the armchair (8, 8) nanotube is a semiconductor with an indirect band gap of 0.20 eV. This gap is smaller than that of the $MoTe_2$ bulk. The valence band edge locates at (0, 0, 0.15), and the conduction band edge locates at (0, 0, 0.325) in fractional units of primitive *k*-vectors.

From the total density of states (TDOS) and the projected DOS on each type of atom, we were able to identify some characteristics of the band structures of the $MoTe_2$ nanotubes. As shown in Figure 4, a main feature of the TDOS is the two well-separated broad peaks below the Fermi level, with a gap of ~3 eV between the two peaks. Near the Fermi level, the TDOS are mainly contributed by the 4d electrons of Mo atoms, whereas the 5p electron Te atoms in both the inner and outer layers give comparable contributions to the TDOS. However, the 5s electrons of Te atoms in the outer layer provide a distinct contribution to the peak in the −10 to −12 eV range. Charge analysis using the Hirshfeld method shows that a small charge is transferred from a Mo atom to a Te atom. For the armchair (8, 8) tube, about 0.038 and 0.054 *e* are transferred to the Te atom in the inner and outer layer, respectively. For the zigzag (10, 0) tube, the charge transfer is about 0.032 and 0.051 *e*. The formation of a tubular structure induces more charge transfer from the Mo atoms to the Te atoms in the outer layer.

Furthermore, we studied a variety of $MoTe_2$ nanotubes with different diameters, ranging from 10 to 17 Å, which included both zigzag (*n*, 0) (*n* = 7, 8, 9, 11, 12, and 13) and armchair (*n*, *n*) (*n* = 4, 5, 6, and 7) nanotubes. The structural information of these nanotubes is summarized in Table 1. The unit-cell length of the periodic supercell in the *c* direction and positions of all atoms were optimized. We note that for the small-diameter zigzag nanotube (7, 0) a stable tubular structure was not achieved. For all armchair nanotubes, the unit-cell length in the *c* direction is about 3.63 Å. For the zigzag nanotubes, the unit-cell length increases slightly with increasing the tube diameter. Meanwhile, the thickness of

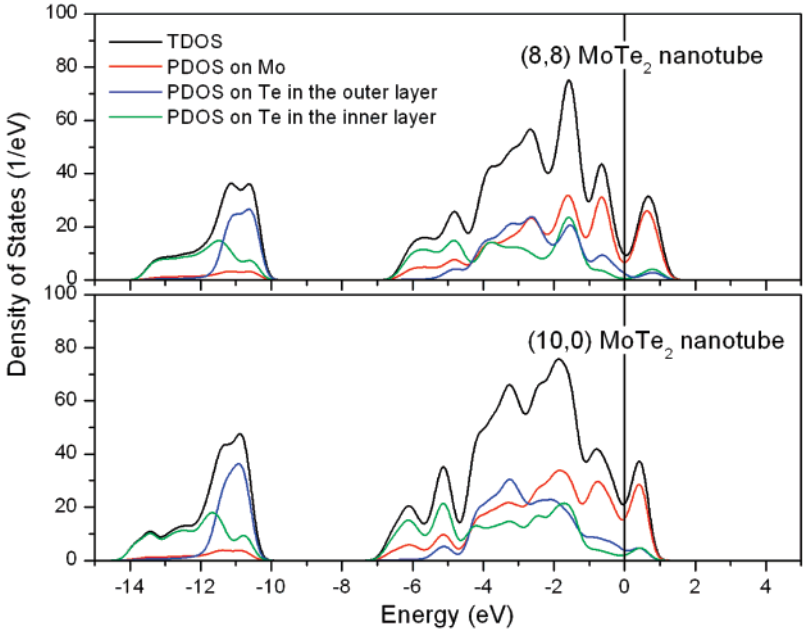

Figure 4. TDOS and PDOS projected on different atomic layers of (10, 0) and (8, 8) $MoTe_2$ nanotubes. The Fermi energy level was set as zero.

Table 1. Diameter of the Nanotube (D), the Wall Thickness (T), the Unit-Cell Length of the Supercell in the c Direction (c), and the Mo−Te Bond Lengths of the Armchair (n, n) (n = 4, 5, 6, 7, and 8) and Zigzag (n, 0) (n = 8, 9, 10, 11, and 12) Nanotubes

nanotube	D (Å)[a]	T (Å)[b]	c (Å)	Mo-Te bond length (Å)
(4, 4)	10.34	3.12	3.63	2.86, 2.74, 2.74,[c] 3.08, 2.85, 2.85[d]
(5, 5)	11.98	3.29	3.63	2.82, 2.75, 2.75, 3.03, 2.83, 2.83
(6, 6)	13.79	3.40	3.63	2.79, 2.74, 2.74, 2.97, 2.83, 2.83
(7, 7)	15.21	3.47	3.63	2.77, 2.73, 2.73, 2.93, 2.82, 2.82
(8, 8)	17.40	3.49	3.63	2.76, 2.74, 2.74, 2.93, 2.81, 2.81
(8, 0)	11.97	3.28	5.58	2.69, 2.82, 2.82, 2.80, 3.00, 3.00
(9, 0)	12.88	3.35	5.80	2.68, 2.79, 2.79, 2.77, 2.97, 2.97
(10, 0)	13.91	3.38	5.88	2.69, 2.78, 2.78, 2.76, 2.95, 2.95
(11, 0)	15.05	3.41	5.91	2.69, 2.77, 2.77, 2.76, 2.93, 2.93
(12, 0)	16.01	3.45	5.97	2.69, 2.77, 2.77, 2.75, 2.92, 2.92
(13, 0)	16.99	3.49	6.00	2.70, 2.77, 2.77, 2.76, 2.90, 2.90
triple-layer in bulk	∞	3.71		2.75

[a] Characterized by the Mo atom in the tube wall. [b] The wall thickness was characterized by the distance between the inner and outer layer. [c] The Mo−Te bonds in the inner layer of the wall. [d] The Mo−Te bonds in the outer layer of the wall.

the wall increases with increasing tube diameter. However, the wall thickness is still less than that of a triple layer (~3.71 Å) in bulk $MoTe_2$. Moreover, the Mo−Te bond lengths decrease as the tube diameter increases. The Mo−Te bonds in the outer layer are longer than those in bulk $MoTe_2$, whereas those in the inner layer can be either elongated or compressed compared to the bulk counterparts, depending on the chirality of the tube as well as the angle between the bond and tube axis. For example, the bonds normal to the axis of a armchair tube are elongated, whereas those not normal to the axis are compressed. But for the zigzag nanotubes, the bonds in the axial direction are compressed, whereas those not in the axial direction are elongated.

In Figure 5, the calculated strain energy per atom was plotted as a function of the tube diameter. The strain energy is defined as the cohesive energy difference between the $MoTe_2$ nanotube and the perfect bulk trilayer structure. As expected, the strain energy decreases with increasing the

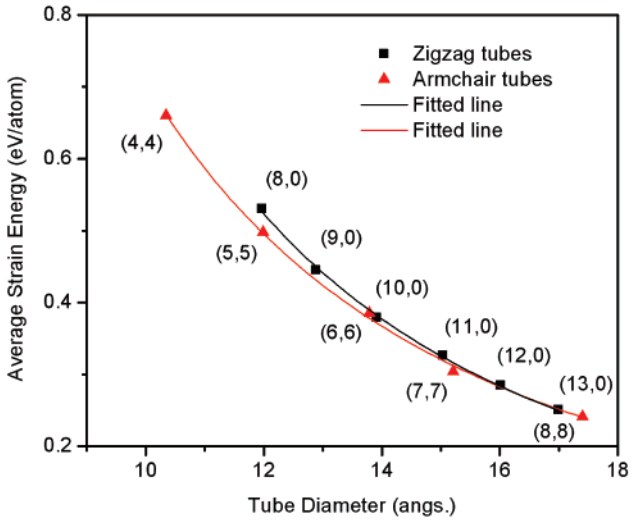

Figure 5. Strain energy per atom vs diameter of $MoTe_2$ nanotubes. Solid lines are fitted with the $1/D^x$ power law, where x is 2.13 and 1.94 for the zigzag and armchair nanotube, respectively.

diameter and is weakly dependent on the chirality. The strain energy follows a $1/D^x$ power law, where x is 2.13 and 1.94 for the zigzag and armchair nanotube, respectively. The armchair nanotube is energetically more favorable than the zigzag nanotube when the diameter of the tube is small. When the diameter is sufficiently large, the strain energy of both zigzag and armchair nanotubes is about the same. Interestingly, the calculated strain energies of $MoTe_2$ nanotubes are smaller than those of MoS_2 nanotubes with the same chirality, suggesting that the formation of $MoTe_2$ nanotubes may be easier than the formation of MoS_2 nanotubes.[49] The band structures of all of the $MoTe_2$ nanotubes considered are calculated, and their band gaps are summarized in Table 2. Clearly, the electronic properties of $MoTe_2$ nanotubes depend on the tube diameter and chirality. In general, the band gap decreases with decreasing the tube diameter, and it is always less than that of bulk $MoTe_2$. $MoTe_2$ nanotubes become metallic or even semimetallic if the diameter is smaller than 16 Å. Large-diameter $MoTe_2$ nanotubes are narrow-gap semiconductors. The armchair nanotubes are indirect semicondutors, whereas the zigzag nanotubes are direct semiconductor. This electronic behavior is similar to that of MoS_2 nanotubes, except that the band gap is less than that of MoS_2 tube having the same chirality. This result suggests that $MoTe_2$ nanotubes may have a higher electrical conductivity than the MoS_2 counterparts.

To further verify structural stabilities of these tubes, we considered both elongated and compressed nanotubes along the axial direction. All of the zigzag nanotubes considered retained their tubular structures in the deformed form. The strain energy increases as the tube is elongated or compressed

Table 2. Calculated Band Gaps of the $MoTe_2$ Nanotubes[a]

nanotube (n, m)	(4, 4)	(5, 5)	(6, 6)	(7, 7)	(8, 8)	(8, 0)	(9, 0)	(10, 0)	(11, 0)	(12, 0)	(13, 0)
direct gap (eV)	0.16	0.50	0.33	0.55	0.80	0.00	0.00	0.00	0.05	0.12	0.21
indirect gap (eV)	0.02	0.00	0.01	0.05	0.20						

[a] The direct band gap is obtained at the gamma (0, 0, 0) point in fractional units of primitive k-vectors.

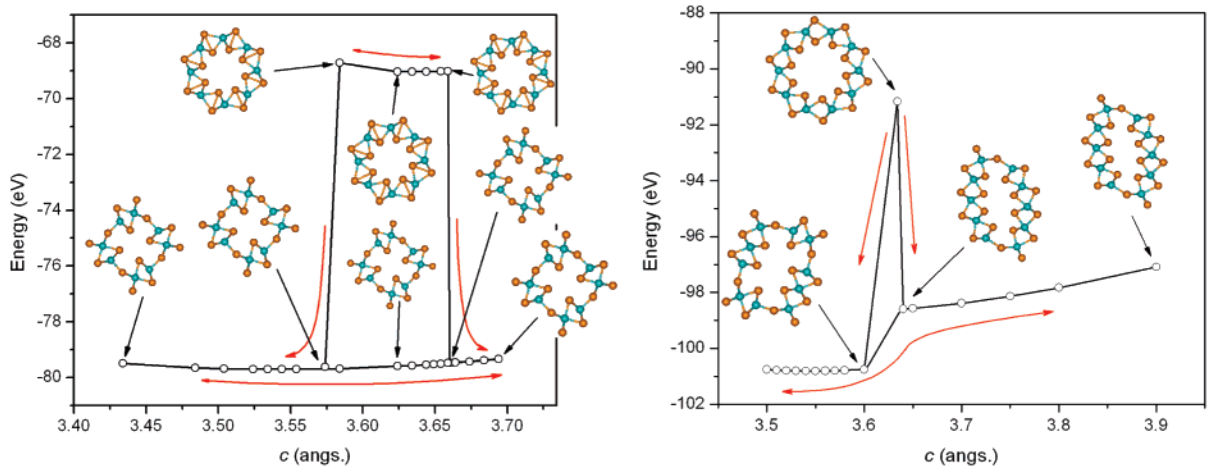

Figure 6. Tubular structures and energy vs length c of the periodic supercell for (4, 4) and (5, 5) $MoTe_2$ nanotubes.

from the optimized geometry. Meanwhile, the electronic properties of the tube are somewhat modified by elongation and compression. For example, the band gaps are reduced slightly or even vanish if the deformation is sufficiently large that it may lead to the semiconductor-to-metal transition. In contrast, the armchair nanotubes exhibit more notable diameter-dependent behavior under the deformation. Although the behavior of large-diameter armchair nanotubes is similar to that of zigzag nanotubes, the behavior of small-dimater armchair nanotubes is much more complex. In Figure 6, the energies and structures of the (4, 4) and (5, 5) nanotubes versus the c length are plotted. The red curves denote either the elongation or compression of the tube. First, we found that the tube structures of (4, 4) and (5, 5) were only marginally stable. Under slight deformation from their equilibrium structure, the tube will collapse and this process is irreversible. The collapsed structures are more-stable than the original tubular structures and their electronic structures are different from those of the original tubes. The collapsed (4, 4) nanotube is a semiconductor with an indirect band gap of ~0.20 eV, and the collapsed (5, 5) nanotube has an indirect band gap of ~0.10 eV, which is closer to that of bulk $MoTe_2$. The structural collapse for small-diameter armchair nanotubes under deformation was seen for $MoTe_2$ nanotubes. It occurs for the armchair (4, 4) MoS_2 nanotube as well. Small-diameter armchair MoS_2 nanotubes have been explored previously, but these nanotubes are either in the rope form or doped with iodine, which may be a reason for observing unstable tube structures.[9,50] Similarly, small-diameter $MoTe_2$ nanotubes may be more stable when forming ropes or/and are doped with foreign atoms.

Finally, the elastic properties of four nanotubes were examined, which included (5, 5), (6, 6), (10, 0), and (11, 0) nanotubes. In addition, the zigzag (18, 0) and armchair (10, 10) CNTs were also considered for comparison. For bulk solids, the Young's modulus is defined as $Y = (\partial^2 E/\partial \epsilon^2)/V_0$, where V_0 is the relaxed equilibrium volume, E is the strain energy per unit cell, and ϵ is the axial strain, defined as c/c_0 where c_0 is the length of the unit cell at mechanical equilibrium. For nanotubes, V_0 can be also defined as the equilibrium volume $V_0 = 2\pi c_0 R l$, where R is the radius and l is the tube thickness. In fact, the definition of tube thickness and Young's modulus is not entirely resolved. For example, the interlayer distance of graphite has been chosen previously as the tube thickness of a single-walled carbon nanotube.[59] In our calculations, we used the same definition as for the thickness (l) of $MoTe_2$, MoS_2, and carbon nanotubes, which is 6.98, 6.15, and 3.4 Å, separately. The calculation results are summarized in Table 3. CNTs have the largest Young's modulus among these tubular systems, whereas the $MoTe_2$ nanotubes are the softest. The Young's modulus of a $MoTe_2$ nanotube is dependent on its diameter and chirality and is reduced slightly as the tube diameter decreases. The Young's modulus of the armchair nanotubes is larger than that of ziagzag nanotubes. Compared with the MoS_2 nanotubes, the $MoTe_2$ nanotubes are much softer because the strain energy per atom of $MoTe_2$ nanotube is smaller than that of MoS_2 nanotube with the same chirality.

Table 3. Calculated Young's Modulus of $MoTe_2$, MoS_2, and Carbon Nanotubes

nanotube	R (Å)	c_0 (Å)	V_0 (Å^3)	$\partial^2E/\partial\epsilon^2$ (eV)	$\partial^2E/(\partial\epsilon^2 \cdot c_0)$ (eV/Å)	Y (GPa)
$MoTe_2$ (6, 6)	6.90	3.63	1098.5	554.0	151.7	80.7
$MoTe_2$ (7, 7)	7.60	3.63	1209.9	635.7	173.9	82.1
$MoTe_2$ (10, 0)	6.96	5.88	1794.8	598.8	101.8	53.4
$MoTe_2$ (11, 0)	7.52	5.91	1949.1	697.9	117.7	57.7
MoS_2 (6, 6)	5.80	3.23	723.9	682.1	211.3	150.8
CNT (10, 10)	6.83	2.47	360.4	2328	942.9	1033.5
CNT (18, 0)	7.09	4.27	646.7	3967	929.9	981.4

Conclusions. We have studied the structure−property relation of single-walled $MoTe_2$ nanotubes using the DFT method. Some general properties of the $MoTe_2$ nanotubes can be summarized as follows: Small-diameter nanotubes are generally less stable than large-diameter nanotubes. All large-diameter nanotubes are narrow-gap semiconductors, and their band gaps decrease with the decrease of tube diameter. In particular, the armchair nanotubes are indirect semiconductors, and the zigzag nanotubes are direct semiconductor. The calculated Young's modulus shows that the $MoTe_2$ nanotubes are relatively soft along the axial direction, and the armchair nanotubes are stiffer than the zigzag

nanotubes. Moreover, the Young's modulus increases with the increase of tube diameter. In closing, it is our hope that this theoretical study will stimulate further experimental studies of the novel $MoTe_2$ nanotubes.

Acknowledgment. We are grateful to valuable discussion with Professor Bruce Parkinson. This work was supported by grants from the DOE's Office of Basic Energy Sciences (DE-FG02-04ER46164), the National Science Foundation (CHE-0427746, CHE-0701540, and CMMI-0709333), the Nebraska Research Initiative, and by the UNL Research Computing Facility.

References

(1) Puotinen, D.; Newnham, R. E. The Crystal Structure of $MoTe_2$. *Acta Crystallogr.* **1961**, *14*, 691.
(2) Kettaf, M.; Conan, A.; Bonnet, A. Electrical Properties of Molybdenum Ditelluride Thin Films. *J. Phys. Chem. Solids* **1990**, *51*, 333.
(3) Balakrishnan, K.; Ramasamy, P. *J. Cryst. Growth* **1994**, *137*, 309.
(4) Vellinga, M.; de Jonge, R.; Haas, C. *J. Solid State Chem.* **1970**, *2*, 299.
(5) Böker, Th.; Severin, R.; Müller, A.; Janowitz, C.; Manzke, R. *Phys. Rev. B* **2001**, *64*, 235305.
(6) Reshak, A. H.; Auluck, S. *Phys. Rev. B* **2005**, *71*, 155114.
(7) Abruña, H. D.; Hope, G. A.; Bard, A. J. *J. Electrochem. Soc.* **1982**, *129*, 2224.
(8) Kiwia, H. L.; Westrum, E. F., Jr. *J. Chem. Thermodyn.* **1975**, *7*, 683.
(9) Remskar, M.; Mrzel, A.; Skraba, Z.; Jesih, A.; Ceh, M.; Demšar, J.; Stadelmann, P.; Lévy, F.; Michailovic, D. *Science* **2001**, *292*, 479.
(10) Ber nède, J. C.; Amory, C.; Assmann, L.; Spiesser, M. *Appl. Surf. Sci.* **2003**, *219*, 238.
(11) Bernède, J. C.; Kettaf, M.; Khelil, A.; Spiesser, M. *Phys. Status Solidi A* **1996**, *157*, 205.
(12) Vellinga, M. B.; De Jonge, R.; Hasa, C *J. Solid State Chem.* **1970**, *2*, 299.
(13) Ajayan, P. M.; Iijima, S. *Nature* **1992**, *358*, 23.
(14) Hamada, N.; Sawada, S.-i.; Oshiyama, A. *Phys. Rev. Lett.* **1992**, *68*, 1579.
(15) Baughman, R. H.; Zakhidov, A. A.; de Heer, W. A. *Science* **2002**, *297*, 787.
(16) Dai, H. J. *Acc. Chem. Res.* **2002**, *35*, 1035.
(17) *Carbon Nanotubes*; Dresselhaus, M. S., Dresselhaus, G., Avouris, Ph., Eds.; Springer: Berlin, 2001.
(18) Rubio, A.; Corkill, J. L.; Cohen, M. L. *Phys. Rev. B* **1994**, *49*, 5081.
(19) Chopra, N. G.; Luyken, R. J.; Cherrey, K.; Crespi, V. H.; Cohen, M. L.; Louie, M. L.; Zettl, A. *Science* **1995**, *269*, 966.
(20) Loiseau, A.; Willaime, F.; Demoncy, N.; Hug, G.; Pascard, H. *Phys. Rev. Lett.* **1996**, *76*, 4737.
(21) Cumings, J.; Zettl, A. *Solid State Comm.* **2004**, *129*, 661.
(22) Tang, C. C.; Bando, Y.; Huang, Y.; Yue, S. L.; Gu, C. Z.; Xu, F. F.; Golberg, D. *J. Am. Chem. Soc.* **2005**, *127*, 6552.
(23) Xie, S. Y.; Kang, W.; Shiral Fernando, K. A.; Wang, X.; Lin, Y.; Sun, Y. P. *Chem. Commun.* **2005**, *29*, 3670.
(24) Ma, R. Z.; Bando, Y.; Zhu, H. W.; Sato, T.; Xu, C. L.; Wu, D. H. *J. Am. Chem. Soc.* **2002**, *124*, 7862.
(25) Tang, C. C.; Bando, Y.; Ding, X. X.; Qi, S. R.; Golberg, D. *J. Am. Chem. Soc.* **2002**, *124*, 14550.
(26) Wu, X. J.; An, W.; Zeng, X. C. *J. Am. Chem. Soc.* **2006**, *128*, 12001.
(27) Wu, X. J.; Yang, J. L.; Zeng, X. C. *J. Chem. Phys.* **2006**, *125*, 44704.
(28) Tenne, R.; Margulis, L.; Genut, M.; Hodes, G. *Nature* **1992**, *360*, 444.
(29) Margulis, L.; Salitra, G.; Tenne, R.; Tallanker, M. *Nature* **1993**, *365*, 113.
(30) Remska, M.; Mrzel, A.; Skraba, Z.; Jesih, A.; Ceh, M.; Demšar, J.; Stadelmann, P.; Lévy, F.; Mihailovic, D. *Science* **2001**, *292*, 479.
(31) Zhu, Y. Q.; Hus, W. K.; Terrones, H.; Grobert, N.; Chang, B. H.; Terrones, M.; Wei, B. Q.; Kroto, H. W.; Walton, D. R. M.; Boothroyd, C. B.; Kinloch, I.; Chen, G. Z.; Windle, A. H.; Fray, D. J. *J. Mater. Chem.* **2000**, *10*, 2570.
(32) Rothschild, A.; Sloan, J.; Tenne, R. *J. Am. Chem. Soc.* **2000**, *122*, 1569.
(33) Nath, M.; Rao, C. N. R. *J. Am. Chem. Soc.* **2001**, *123*, 4841.
(34) Rosenfeld Hacohen, Y.; Grunbaum, E.; Tenne, R.; Sloan, J.; Hutchison, J. L. *Nature* **1998**, *395*, 336.
(35) Hong, S. Y.; Popovitz-Biro, R.; Prior, Y.; Tenne, R. *J. Am. Chem. Soc.* **2003**, *125*, 10470.
(36) Nath, M.; Rao, C. N. R. *Angew. Chem., Int. Ed.* **2002**, *41*, 3451.
(37) Ajayan, P. M.; Stephan, O.; Redlich, Ph.; Colliex, C. *Nature* **1995**, *375*, 564.
(38) Rao, C. N. R.; Govindaraj, A.; Leonard Deepak, F.; Gunari, N. A.; Nath, M. *Appl. Phys. Lett.* **2001**, *78*, 1853.
(39) Kasuga, T.; Hiramatsu, M.; Hoson, A.; Sekino, T.; Niihara, K. *Adv. Mater.* **1999**, *11*, 1307.
(40) Tian, Z. R.; Voigv, J. A.; Liu, J.; Mckenzie, B.; Xu, H. F. *J. Am. Chem. Soc.* **2003**, *125*, 12384.
(41) Rothschild, A.; Cohen, S. R.; Tenne, R. *Appl. Phys. Lett.* **1999**, *75*, 4025.
(42) Côté, M.; Cohen, M. L.; Chadi, D. J. *Phys. Rev. B* **1998**, *58*, R4277.
(43) Chang, H.; In, E.; Kong, K.-j.; Lee, J.-O.; Choi, Y.; Ryu, B.-H. *J. Phys. Chem. B* **2005**, *109*, 30.
(44) Rapoport, L.; Bilik, Y.; Feldman, Y.; Homyonfer, M.; Cohen, S. R.; Tenne, R. *Nature* **1997**, *387*, 791.
(45) Golan, Y.; Drummond, C.; Homyonfer, M.; Feldman, Y.; Tenne, R.; Israelachvili, J. *Adv. Mater.* **1999**, *11*, 934.
(46) Chhowalla, M.; Amaratunga, G. A. J. *Nature* **2000**, *407*, 164.
(47) Chen, J.; Kuriyama, N.; Yuan, H.; Takeshita, H. T.; Sakai, T. *J. Am. Chem. Soc.* **2001**, *123*, 11813.
(48) Kaplan-Ashiri, I.; Cohen, S. R.; Gartsman, K.; Ivanovskaya, V.; Heine, T.; Seifert, G.; Wiesel, I.; Wagner, H. D.; Tenne, R. *Proc. Natl. Acad. Sci U.S.A.* **2006**, *103*, 523.
(49) Seifert, G.; Terrones, H.; Terrones, M.; Jungnickel, G.; Frauenheim, T. *Phys. Rev. Lett.* **2000**, *85*, 146.
(50) Verstraete, M.; Charlier, J.-C. *Phys. Rev. B* **2003**, *68*, 45423.
(51) Galván, D. H.; Rangel, R.; Adem, E. *Fullerene Sci. Technol.* **1999**, *7*, 421.
(52) Flores, E.; Tlahuice, A.; Adem. E.; Galván, D. H. *Fullerene Sci. Technol.* **2001**, *9*, 9.
(53) Qiu, L. H.; Pol. V. G.; Wei, Y.; Gedanken, A. *J. Mater. Chem.* **2003**, *13*, 2985.
(54) (a) Delley, B. *J. Chem. Phys.* **1990**, *92*, 508. (b) Delley, B. *J. Chem Phys.* **2003**, *113*, 7756. DMol3 is available from Accelrys.
(55) Perdew, J. P.; Burke, K.; Ernzerhof, M. *Phys. Rev. Lett.* **1996**, *77*, 3865.
(56) Hehre, W. J.; Radom, L.; Schlyer, P. v. R.; Pople, J. A. *Ab initio Molecular Orbital Theory*; Wiley: New York, 1986.
(57) Delley, B. *Phys. Rev. B* **2002**, *66*, 155125.
(58) Monkhorst, H. J.; Pack, J. D. *Phys. Rev. B* **1976**, *13*, 5188.
(59) Lu, J. P. *Phys. Rev. Lett.* **1999**, *79*, 1297.

NL071165+